FULL PAPER

Optical Fiber Sensors

ADVANCED
OPTICAL
MATERIALS
www.advopticalmat.d

Excitation of Bloch Surface Waves on an Optical Fiber Tip

Michele Scaravilli, Alberto Micco, Giuseppe Castaldi, Giuseppe Coppola, Mariano Gioffrè, Mario Iodice, Vera La Ferrara, Vincenzo Galdi,* and Andrea Cusano*

The integration of structures supporting Bloch surface waves (BSWs) with optical fibers is highly desirable, since it would enable the development of high-figure-of-merit miniaturized all-fiber optrodes, opening new pathways within the "lab-on-fiber" roadmap. Here, the first experimental demonstration of grating-assisted excitation of BSWs on the tip of single-mode fibers in the near-infrared region is provided. This is attained via fabrication of a 1D diffraction grating on the fiber facet, and subsequent deposition of a 1D photonic crystal. In spite of a resonance broadening due to grating-induced morphological perturbations, the measured Q-factor of 50 is still higher than typical lab-on-tip plasmonic-probe benchmarks. With a view toward biomolecular sensing, a surface sensitivity of 1.22 nm nm^{-1} of homogeneous overlay deposited over the active region, which is in line with most plasmonic optrodes largely used in connection with optical fibers, is evaluated. The results also highlight the current limitations and the challenges to face for the development of advanced BSW-based fiber-tip platforms for biological sensing applications.

1. Introduction

Photonic devices based on surface waves (SWs) are inherently apt for label-free chemical and biochemical detections of target analytes, due to the strong interaction attainable between subwavelength-localized electromagnetic fields and the surrounding environment.[1]

Although the theoretical investigation of SW propagation began more than a century ago,[2] only one type of SW, the surface plasmon polariton (SPP), dominates the state of the art.[1,3] Indeed, the remarkable probing capabilities of SPPs have led

to the development of extremely sensitive surface plasmon resonance (SPR) biosensors, which can rely on mature fabrication technologies, standard biofunctionalization protocols, and commercial scale production.[1,3–5] In spite of the excellent performance achieved by state-of-the-art SPR platforms, with reported limits of detection (LODs) approaching 10^{-7} refractive index units (RIU),[4,6] further improvements are unavoidably limited by the reliance on lossy materials (typically metals). This yields an undesirable resonance broadening, thereby posing an upper bound to the overall figure of merit (FOM).[6] For this reason, there is a strong push to explore alternative, larger-FOM SW implementations.[1,7–11]

As a prominent example, Bloch SWs (BSWs) on truncated 1D photonic crystals (1DPCs) represent an attractive alternative to SPPs, as recently demonstrated in several proof-of-principle studies.[9,12–16] In spite of sensitivities to local refractive index (RI) changes lower than SPR platforms, the completely dielectric low-loss structure of a BSW sensor yields sensibly sharper resonances, leading to generally larger FOMs.[13–17] This has recently led to the successful development of label-free biosensors exhibiting competitive performance in practical biomolecular detections.[18–25] Moreover, BSW structures offer further benefits with respect to other SW-based counterparts, such as easy realization and experimental observation, and great flexibility in terms of wavelength range of operation, materials choice, and tailoring of the field distribution for specific sensing applications.[1,9,13–15,17,26–28]

While most sensing platforms proposed in the literature rely on bulky prism-coupled planar configurations,[12–26] the integration of BSW structures with optical fibers would bring significant benefits in terms of compactness, light weight, remote sensing capability, biocompatibility, and ease of interrogation. This is especially attractive within the emerging "lab-on-fiber" technology framework.[29–34] The interest in this topic has started growing within the last two years, as witnessed by theoretical studies of BSW sensors based on the use of D-type fibers,[35] and unclad regions of multimode fibers.[36] A first experimental demonstration on a tapered single-mode fiber has also been provided very recently.[37] Within this context, a more intriguing scenario is represented by the integration of the resonant structure directly on the fiber tip. This would allow exploiting fabrication methodologies typically adopted for photonic biochips, thereby enabling the development of probes

Dr. M. Scaravilli, Dr. A. Micco, Prof. G. Castaldi, Prof. V. Galdi, Prof. A. Cusano
Department of Engineering
University of Sannio
I-82100 Benevento, Italy
E-mail: vgaldi@unisannio.it; a.cusano@unisannio.it
Dr. G. Coppola, Dr. M. Gioffrè, Dr. M. Iodice
Institute for Microelectronics and Microsystems
National Research Council
I-80131 Napoli, Italy
Dr. V. La Ferrara
ENEA
Portici Research Center
I-80055 Portici, Napoli, Italy

The ORCID identification number(s) for the author(s) of this article can be found under https://doi.org/10.1002/adom.201800477.

with even higher levels of miniaturization and great potentials for in vivo applications.[30–32] Against a background of "lab-on-tip" devices typically based on plasmonic nanostructures,[30–32] "all-dielectric" SW fiber tip structures could yield dramatic LOD improvements, while still relying on already available interrogation systems. Therefore, the possibility to effectively realize a strongly sensitive high-Q lab-on-tip platform would clearly represent an important milestone within the lab-on-fiber technology roadmap.

The above examples of on-fiber integration of BSW structures do not involve the fiber facet. This is due to the paramount hurdle of the excitation of a BSW at the surface of a 1DPC deposited on the tip of either a single-mode fiber (with the light beam normally incident) or a multimode fiber (with poor control of the coupling conditions). In a recent study,[28] we theoretically showed the possibility to achieve on-tip excitation in a single-mode fiber via grating coupling. Building up on these results, in this study, we proceed with the experimental validation, by exploring the practical realization of the two grating-coupled platforms previously introduced in ref. [28].

2. Results and Discussion

2.1. Surface-Diffraction-Grating Configuration

We start considering the configuration schematized in **Figure 1**a.[28] A 1D diffraction grating (1DDG) made of $2N$ alternating layers of silicon nitride (Si_3N_4, $n_1 = 1.73$) and silica (SiO_2, $n_2 \approx 1.46$) (with thicknesses d_1 and d_2, respectively) is deposited on the tip of a single-mode optical fiber (fused silica, $n_{inc} = 1.45$). An additional Si_3N_4 layer of thickness d_{term} terminates the 1DPC and is periodically patterned in order to obtain a 1DDG (with period Λ, height h, and duty cycle DC). This enables the excitation of a BSW at the undulated interface between the 1DPC and the external medium, assumed as air ($n_{ext} = 1$).[28] The RIs of the two materials were measured via ellipsometric characterizations of layers deposited via radio frequency (RF) magnetron sputtering on glass substrates, whereas the extinction coefficients could not be accurately measured (see the Supporting Information for details).

The geometrical parameters of the structure were dimensioned according to the design procedure in ref. [28], aided by full-wave rigorous coupled-wave approach (RCWA) simulations[38,39] (see the Supporting Information). Specifically, by assuming a plane wave with transverse-electric (TE) polarization (y-directed electric field) normally impinging at the fiber tip, and lossless materials in the 1DPC, we obtained: $d_1 = 350$ nm, $d_2 = 760$ nm, $d_{term} = 130$ nm, $N = 8$, $\Lambda = 1180$ nm, $h = 30$ nm, and DC = 0.5. As shown in Figure 1b, a BSW resonance arises in the zeroth-order reflectance spectrum around the wavelength $\lambda = 1572$ nm, with high visibility (peak/dip excursion $H \approx 0.8$) and narrow bandwidth. We evaluated a linewidth $\Gamma \approx 0.194$ nm (Q-factor of ≈ 8100) by adopting a numerical fitting method based on the Breit–Wigner–Fano formula.[40] The field at the resonance wavelength is tightly confined at the 1DPC surface, as it can be observed in Figure 1c.

We deposited the required 17-layer Si_3N_4/SiO_2 1DPC on the cleaved end of single-mode fibers by means of a sputtering technique specifically optimized for an "unconventional" substrate such as the fiber tip (see the Supporting Information for details).

After fabricating three 1DPC-coated samples according to the design specifications above, we realized the required periodic pattern on their surface via a focused ion beam (FIB) milling method, already successfully utilized for fabricating fiber-tip plasmonic/photonic resonant nanostructures such as "double-layer" photonic-crystal slabs,[41] plasmonic metasurfaces,[33] and microgel-coated metal hole arrays.[42] As a result, a square area of 47.2 μm × 47.2 μm was patterned around the core region of each sample, giving rise to a 1DDG with 40 periods. Scanning electron microscope (SEM) images of a sample are shown in **Figure 2**a,b.

Spectral characterizations of the realized samples (see the Supporting Information for details and results for each fabricated sample) did not show the excitation of the expected BSW resonance, or polarization dependence of the collected spectra in the wavelength range of investigation. For example, Figure 2c,d shows the spectrum retrieved from one sample and its numerical counterparts (for various values of the extinction coefficients), respectively.

The significant disagreement between the numerical and experimental outcomes may originate from three nonideality effects, whose interplay may inhibit the observation of the expected resonant phenomenon: (i) absorption in the layers of the 1DPC; (ii) finite size of the 1DDG; (iii) reduced efficiency of the grating coupling phenomenon.

The influence of optical losses in the 1DPC on the spectral characteristics of a BSW resonance has been previously discussed in ref. [28] and is summarized in Figure 2d for the case of interest. In particular, we show the results of simulations also taking into account nonzero values of the extinction coefficients κ_1 and κ_2 pertaining to the Si_3N_4 and SiO_2 layers, respectively. As it can be observed, absorption in the 1DPC induces a significant degradation of the resonant lineshape by comparison with the lossless case. Specifically, a 62.5% visibility decrease is already noticeable for $\kappa_{1,2} = 10^{-4}$, while the BSW excitation yields only a shallow dip around the operational wavelength for $\kappa_{1,2} = 10^{-3}$. For this reason, we fabricated and characterized another set of samples according to an alternative design strategy, conceived with the primary goal of strongly increasing the robustness of the arising resonance against extinction coefficients as high as 10^{-3} (see the Supporting Information for details). Also in this case, we did not observe the expected resonance in any of the retrieved reflectance spectra. This excludes the possibility of a key role played by the above effect.

The finite size of the 1DDG, not accounted for in our numerical model, may also explain the discrepancies. Indeed, on one hand, only a limited number of grating periods interact with the impinging beam, thereby reducing the coupling efficiency. In particular, in the fabricated structures, only eight periods are encompassed within the mode-field diameter of the single-mode fiber (≈10 μm at 1550 nm). On the other hand, finite-size effects may limit the efficiency of light collection if the size of the grating region is not suitable to confine the in-plane extension of the coupled mode.[43] Within this context, successful observations of spectral resonances in many lab-on-tip plasmonic structures[29,33,42,44–46] can be attributed to the
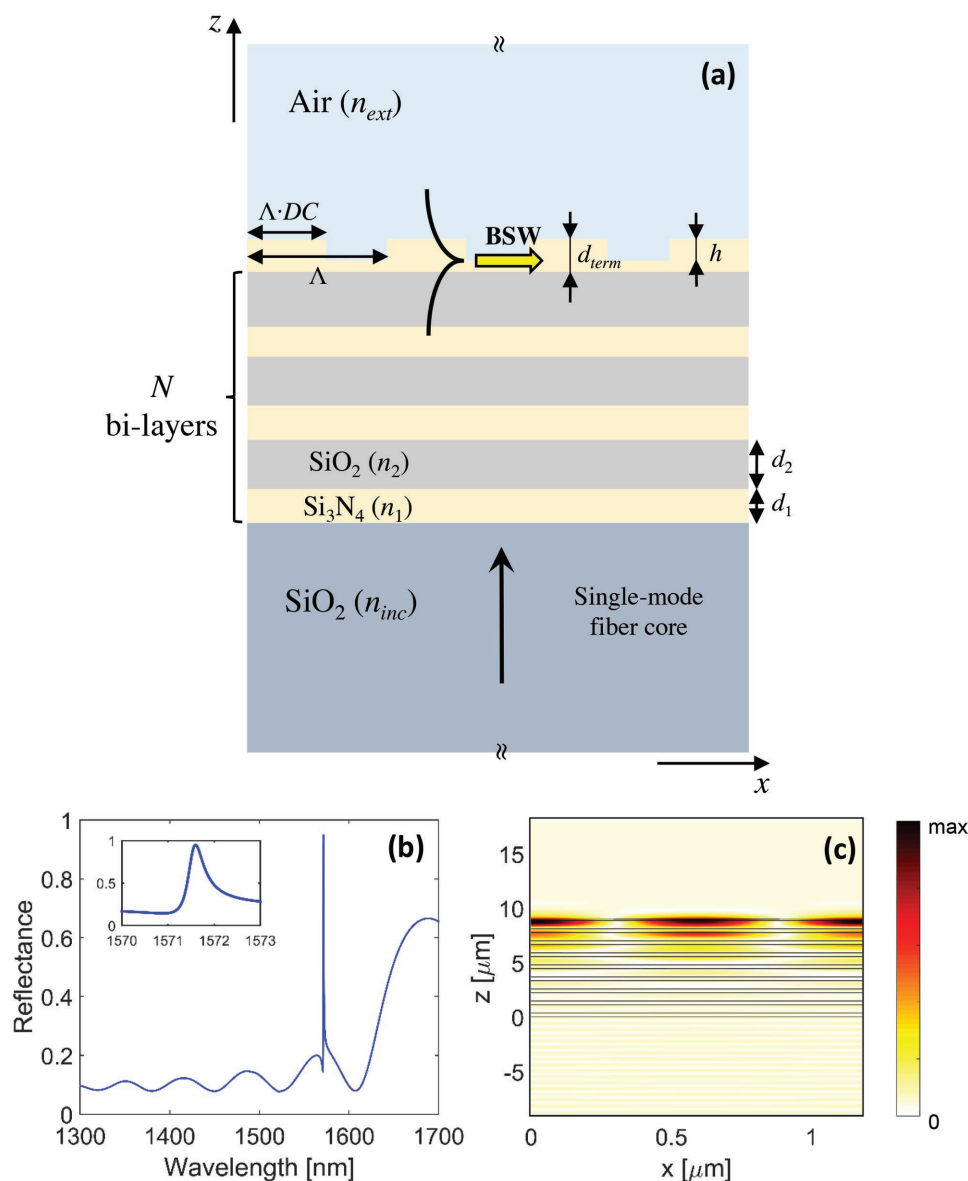
Figure 1. a) 2D schematic of the surface diffraction grating configuration in the (x–z) reference system. Geometrical parameters and field quantities are assumed as invariant along the y-axis. The tip of a single-mode optical fiber is coated with a N-period 1DPC, whose unit cell is made of two layers of Si_3N_4 and SiO_2 of thickness d_1 and d_2, respectively. A Si_3N_4 termination layer of thickness d_{term} is placed on the top of the 1DPC. A 1DDG (with period Λ, height h, and duty cycle DC) is written on the termination layer, in order to couple a BSW at its undulated surface. The outer environment is assumed as air. b) Zeroth-order reflectance spectrum for TE polarization, computed for a structure with $d_1 = 350$ nm, $d_2 = 760$ nm, $d_{term} = 130$ nm, $N = 8$, $\Lambda = 1180$ nm, $h = 30$ nm, and DC = 0.5. The spectral region around the BSW resonance is magnified in the inset. c) Magnitude map of the electric field within a unit cell, evaluated at the wavelength $\lambda = 1572$ nm.

excitation of localized modes, well confined within the grating boundary. A related study was carried out in ref. [44], where a gradual reduction of the active region of a metallo-dielectric plasmonic nanostructure from the entire cladding area down to a square area of 20 μm × 20 μm did not yield substantial variations in the retrieved spectral features, revealing a good robustness of the structure against finite-size effects. Nevertheless, "edge" effects are known to strongly limit the outcoupling process in dielectric structures supporting high-Q propagating modes, with detrimental influence on the resonance visibility and bandwidth, as discussed and observed for both planar[43]

and fiber-tip[41] photonic resonators. In our case, if the BSW is not efficiently enclosed within the patterned area on the fiber tip, unavoidable losses are expected, due to both scattering at the discontinuity and coupling to BSWs sustained by the planar 1DPC surface outside the grating boundary. This may have a potentially severe impact on the actual observability of the BSW resonance.

Also prominent among the unmodeled effects is the assumption, in our numerical modeling, of plane-wave excitation instead of a fiber mode. For other lab-on-fiber configurations,[44] this approximation was found to provide acceptably
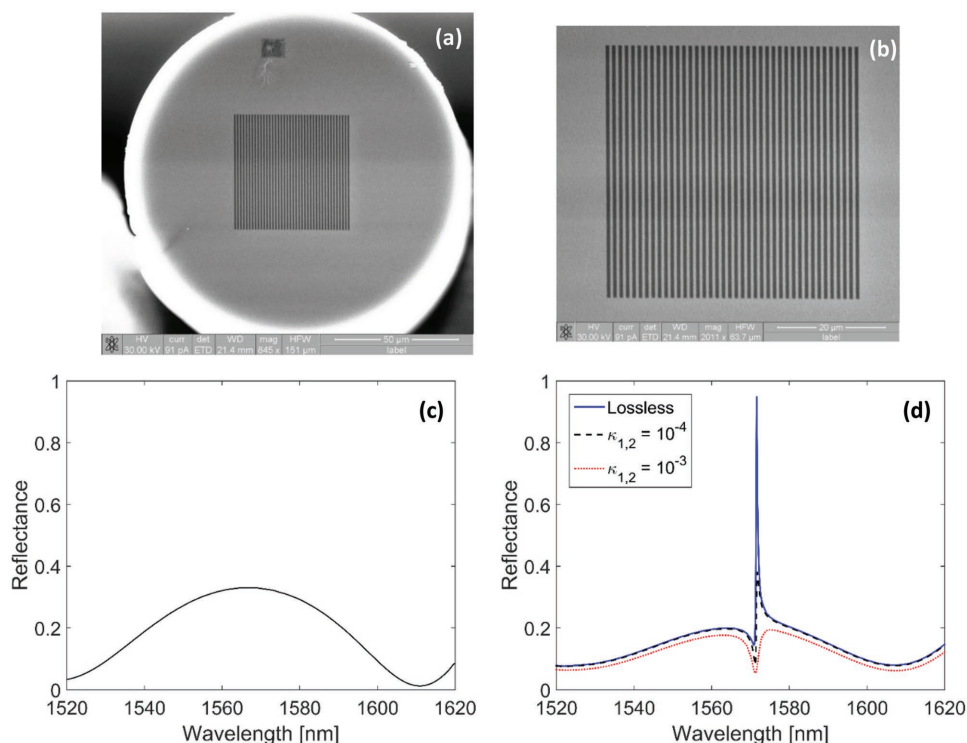
ADVANCED
SCIENCE NEWS
www.advancedsciencenews.com

ADVANCED
OPTICAL
MATERIALS
www.advopticalmat.de

Figure 2. a) SEM image of a sample fabricated according to the design parameters in Figure 1b. More specifically, a periodic array of strips is patterned on the surface of a predeposited 1DPC within a square area of 47.2 μm × 47.2 μm around the core region. b) Magnification of the fabricated 1DDG. c) Measured reflectance spectrum for one sample, not exhibiting any polarization-induced variation. d) Numerical zeroth-order reflectance spectrum for TE polarization, computed for different values of the extinction coefficients κ_1 and κ_2.

accurate results, with only slight blueshifts and reduced visibility of the resonant lineshapes. In the present configuration, the light beam emerging from the fiber tip exhibits an unmodeled angular spreading, and propagates for a long path (several μm) before impinging on the grating, undergoing optical losses due to oblique-angle reflections/transmissions at the interfaces between the layers of the 1DPC. Therefore, a weakened interaction between the light normally impinging at the 1DPC termination and the grating occurs at the resonance wavelength, with a consequent decrease of the coupling efficiency with the BSW. In a complementary way, the above effects are expected to also play a role in further lowering the amount of light collected in the core. In what follows, we explore an alternative configuration, which potentially overcomes this last issue.

2.2. On-Tip Diffraction-Grating Configuration

In order to elucidate the role played by the reduced light/grating interaction, we investigated an alternative grating-coupled configuration, based on the direct writing of a deep 1DDG on the fiber tip. This choice allows enhancing the resonantly scattered power with respect to the previous configuration, and partially mitigating finite-size effects (which are significant for weakly diffractive structures[43]).

The idealized BSW structure under analysis (theoretically studied in ref. [28]) is schematized in **Figure 3**a. Specifically, we engineered the parameter configuration in order to obtain

a fairly narrow resonance, while limiting the effect of dielectric losses in the 1DPC. Following ref. [28], we enforced the coupling of the BSW near the cut-off condition, in order to minimize the field content in the 1DPC. Figure 3b shows the zeroth-order reflectance spectrum (blue curve) for TE-polarization and a structure with $d_1 = 275$ nm, $d_2 = 370$ nm, $d_{\text{term}} = 390$ nm, $N = 6$, $\Lambda = 1540$ nm, $h = 600$ nm, and DC = 0.5. The spectrum exhibits a resonance around $\lambda \approx 1550$ nm, with $\Gamma \approx 2.2$ nm ($Q \approx 705$) and negligible influence of the extinction coefficients $\kappa_{1,2} = 10^{-3}$ (red-dotted curve). As a consequence of the design procedure, a strong enhancement of the BSW resonant field distribution in the external medium is attained, as shown in Figure 3c.

However, as discussed in ref. [28], the optical response of the structure is expected to suffer from the expectable fabrication-related "propagation" of the undulated profile of the substrate on the subsequently deposited layers of the 1DPC. As a proof of this concept, Figure 3d shows the TE spectral response (blue curve) obtained in the worst case, that is, by considering a structure in which all the layers of the 1DPC exhibit a periodic undulation characterized by same height, period, and duty cycle of the original grating. The structure is weakly sensitive to optical losses in the 1DPC (see red-dotted curve, evaluated for $\kappa_{1,2} = 10^{-3}$). However, by comparison with Figure 3b, the arising resonant dip undergoes an ≈150 nm redshift and is now located at $\lambda \approx 1680$ nm. Moreover, it exhibits a sensible broadening of more than one order of magnitude ($\Gamma \approx 80$ nm) by comparison with the idealized case (no propagation of the
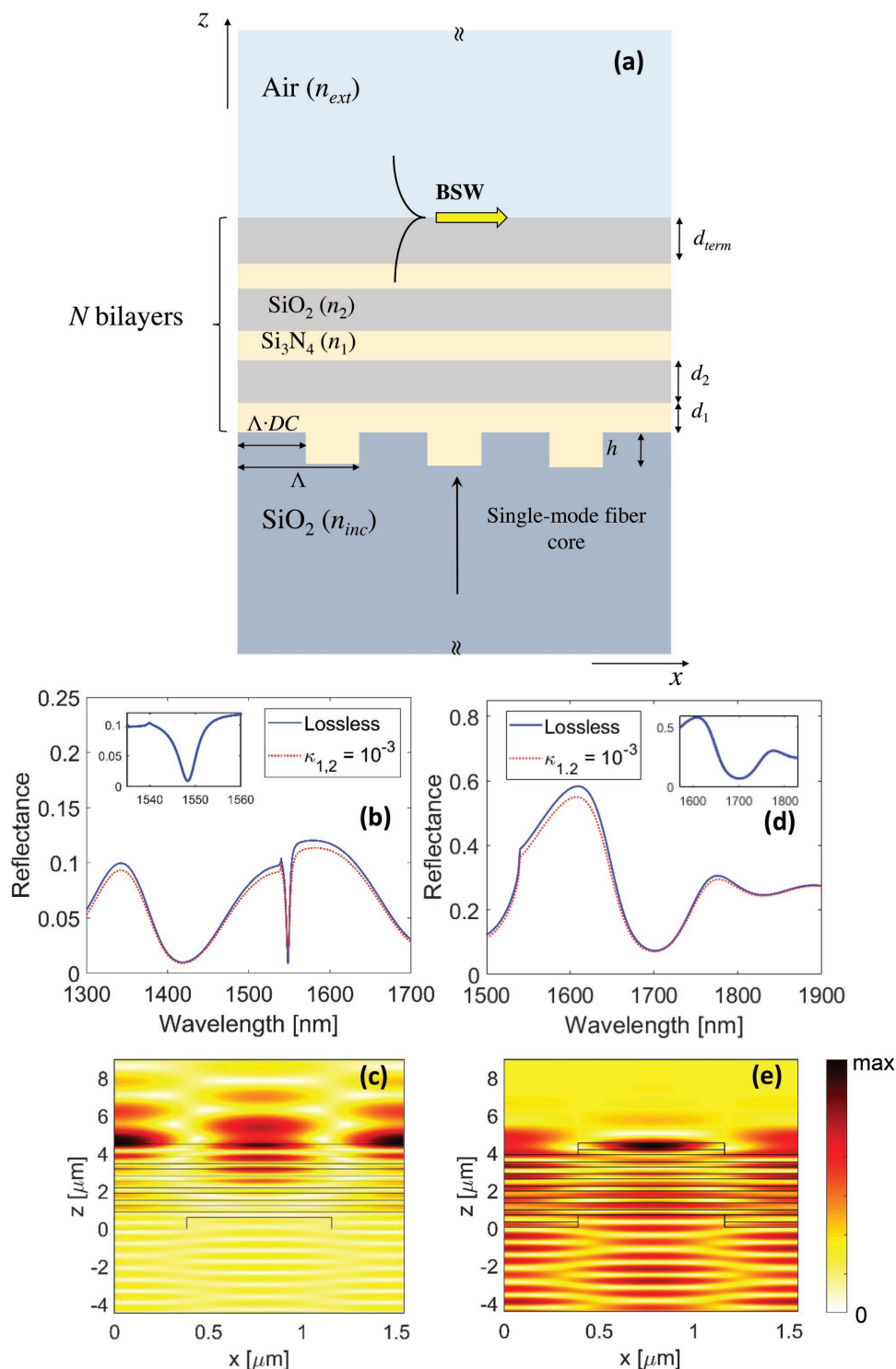
Figure 3. a) As in Figure 1a, but for the on-tip diffraction grating (idealized) configuration. The tip of a single-mode optical fiber is coated with a $N-1$-period 1DPC, whose unit cell is made of two layers of Si_3N_4 and SiO_2 of thickness d_1 and d_2, respectively. A bilayer composed of a Si_3N_4 layer (with thickness d_1) and a SiO_2 layer of thickness d_{term} terminates the 1DPC. A 1DDG (with period Λ, height h, and duty cycle DC) is written on the fiber tip (at the bottom of the 1DPC) in order to couple a BSW at the surface of the 1DPC. b) Zeroth-order reflectance spectrum for TE polarization, pertaining to a structure with $d_1 = 275$ nm, $d_2 = 370$ nm, $d_{term} = 390$ nm, $N = 6$, $\Lambda = 1540$ nm, $h = 600$ nm, and DC = 0.5, computed in the lossless case and for $\kappa_{1,2} = 10^{-3}$. The spectral region around the BSW resonance is magnified in the inset. c) Corresponding magnitude map of the electric field within a unit cell, evaluated at the wavelength $\lambda = 1550$ nm for $\kappa_{1,2} = 0$. d) Same as panel (b), but considering the relief-propagation effects: all layers of the 1DPC are assumed to exhibit a periodic surface profile, modeled with a square wave with period Λ, duty cycle DC, and height h. e) Corresponding magnitude map of the electric field within a unit cell, evaluated at the wavelength $\lambda = 1680$ nm for $\kappa_{1,2} = 0$.

**ADVANCED
SCIENCE NEWS**

www.advancedsciencenews.com

**ADVANCED
OPTICAL
MATERIALS**
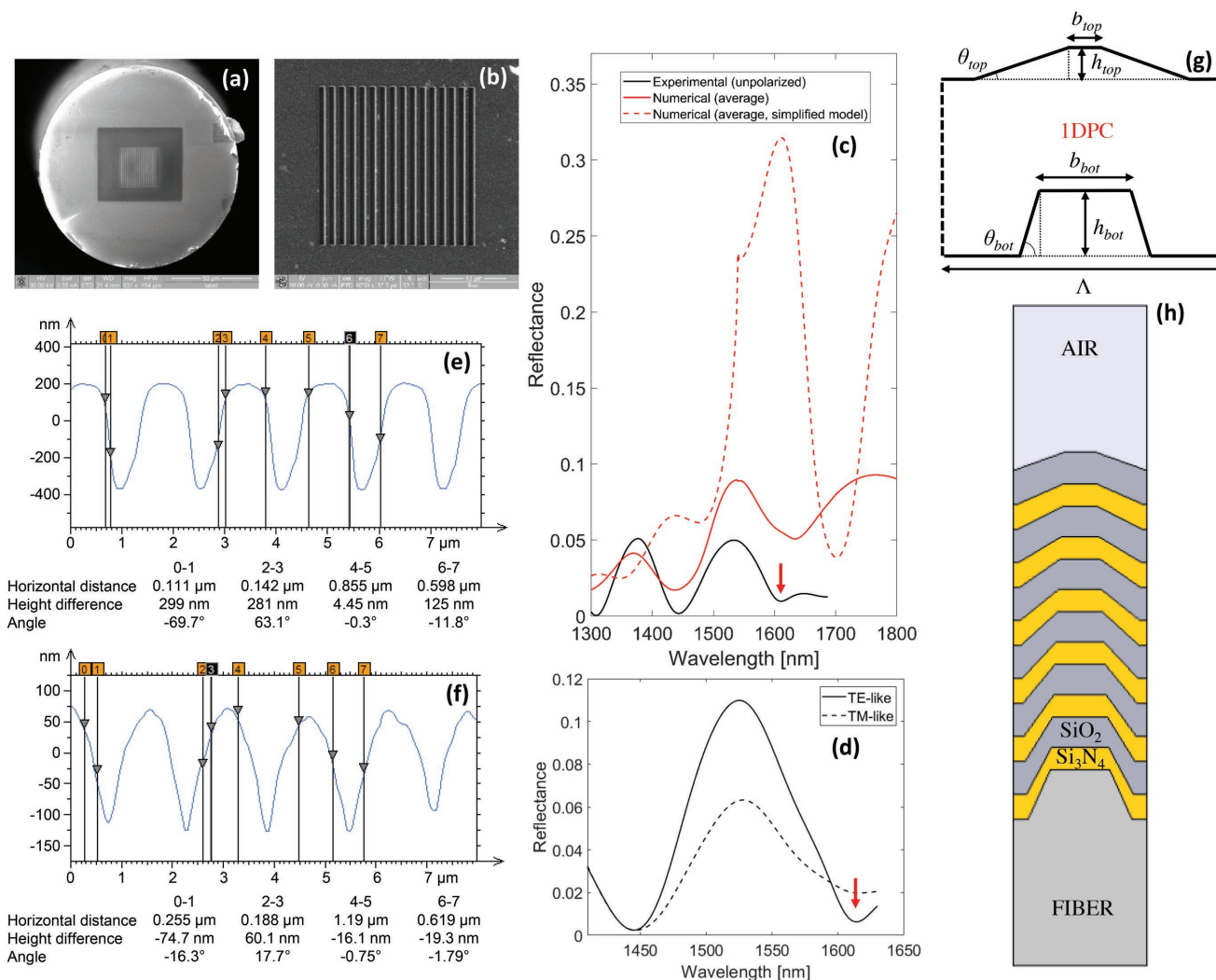
www.advopticalmat.de

Figure 4. a) SEM image of a fiber tip after writing a 1DDG according to the design parameters in Figure 3b. More specifically, a periodic array of strips is patterned on the fiber glass within a square area of 23.1 µm × 23.1 µm around the core region, after removing a sacrificial 50 nm thick gold layer on an area of ≈40 µm × 40 µm. The nonmilled region is still covered by gold (see the Supporting Information for more details). b) Magnification of the fabricated 1DDG. c) Comparison among: experimental reflectance spectrum acquired with an unpolarized source after a selective removal of the remaining gold on the fiber facet and the subsequent deposition of a 1DPC with parameters as in Figure 3b (black curve), numerical spectrum (averaged over TE and TM polarizations) of the structure in Figure 3d,e (red-dashed curve); numerical (average) spectrum pertaining to the structure in panel (h) (red-solid curve). d) Experimental reflectance spectra acquired with a polarized source, for TE-like and TM-like polarizations. e) AFM profile pertaining to a 1D periodic pattern of strips with nominal parameters as in Figure 3b written on the fiber tip, evaluated along a scan line parallel to the periodicity axis of the pattern. The measurements of some geometrical parameters are indicated. f) Same as panel (e), but referred to the surface of the 1DPC deposited on the templated tip. g) Schematic of the unit cell of the structure considered for the fitting of the experimental data, with $h_{bot} = 577$ nm, $b_{bot} = 685$ nm, $\theta_{bot} = 66°$, $h_{top} = 207$ nm, $b_{top} = 350$ nm, and $\theta_{top} = 17°$. The geometrical parameters take into account the information provided by the AFM measurements in panels (e) and (f). h) Unit cell of the geometry simulated with COMSOL Multiphysics.

undulated profile), and is accompanied by a poor field enhancement around the 1DPC/air interface (Figure 3e).

Acknowledging this unavoidable degradation, we fabricated the described structure, with the primary goals of (i) verifying the possibility to couple a BSW via mitigation of the drawbacks of the surface-diffraction-grating configuration, and (ii) experimentally evaluating the effective degree of relief-propagation on a 1DPC deposited on the fiber tip. In particular, we fabricated the required 1DDG on the tip of three fibers. For each sample, a 15 period grating was written within a square area of 23.1 µm × 23.1 µm around the core region (see SEM images

in **Figure** 4a,b). The subsequent deposition of the required 12-layer Si3N4/SiO2 1DPC was carried out on two samples, with the third one left uncoated so as to enable morphological measurements (as described hereafter).

For the experimental characterization, we utilized a supercontinuum source, emitting unpolarized light in a broad bandwidth (see the Supporting Information for further details). The outcome of the optical characterization pertaining to a reference sample is shown in Figure 4c (black curve). The spectrum retrieved from the other sample is shown in the Supporting Information. As it can be observed, a rather broad dip (indicated

ADVANCED
SCIENCE NEWS
www.advancedsciencenews.com

ADVANCED
OPTICAL
MATERIALS
www.advopticalmat.de

by a red arrow) arises in the spectral region of interest around $\lambda \approx 1611$ nm, redshifted by comparison with the idealized case. This behavior is qualitatively in line with the outcomes of the previous numerical analysis (see Figure 3b,d). To account for the unpolarized character of the excitation in our numerical model (red-dashed curve), we averaged the responses for transverse-magnetic (TM, i.e., y-directed magnetic field) and TE polarization. Significant differences in terms of (i) wavelength position of the dips, (ii) reflectance values, and (iii) shapes of the Fabry–Perot envelopes are noticeable.

Nevertheless, the presence of a BSW coupling phenomenon at the above mentioned dip is confirmed by the results of polarization measurements, summarized in Figure 4d for the reference sample (see the Supporting Information for further details). As theoretically expected, the dip exhibits a strong polarization-dependent shape, reaching its maximum and minimum visibility for light polarization states that can be identified as "TE-like" (black-solid curve) and "TM-like" (black-dashed curve), respectively. As it will be more evident in the following, the highlighted spectral feature corresponds indeed to a BSW resonance, degraded by the relief-propagation phenomenon.

To better elucidate the above effects, we carried out some morphological measurements, which enabled a quantitative evaluation of the degree of perturbation of the 1DPC morphology induced by the templated fiber tip. More specifically, we analyzed the fabricated samples via surface profile measurements with an atomic force microscope (AFM, see the Supporting Information). As a first step, we investigated the aforementioned uncoated FIB-milled tip, and accurately evaluated its geometrical parameters. Figure 4e shows the 1DDG profile along a scan line parallel to the periodicity axis and some results of the measurements (see the Supporting Information for AFM images of the pattern). As expected,[41] the profile is pseudo-trapezoidal. This effect is inherent of the FIB patterning process, which leads to an array of strips nonuniform along their depth, that is, wider than the nominal width $\Lambda (1 - DC) = 770$ nm on the top, and narrower on the bottom. Specifically, the strips have a width of ≈ 855 nm on the surface of the pattern and oblique sidewalls, inclined by an angle of $\approx 24°$ with respect to direction normal to the scanned plane (see Figure 4e and the Supporting Information). We found a very good compliance with the design constraints for the height (with a maximum measured value of ≈ 577 nm) and the period (≈ 1540 nm).

We carried out the same analysis for the surface of the 1DPC pertaining to the reference sample. As it can be observed in Figure 4f, despite the sequential deposition of 12 layers on the templated tip, a periodic undulation still arises on the SiO_2 termination layer. In particular, the surface pattern exhibits a triangular smoothed profile, preserving the original periodicity (≈ 1540 nm measured period). Specifically, the strips have a width of ≈ 1190 nm on the top, and are characterized by strongly inclined sidewalls, forming an angle of $\approx 73°$ with respect to the direction normal to the scanned plane (see Figure 4d). The measured height (maximum value of ≈ 207 nm) is about one-third of the value measured on the fiber tip.

The above measurements indicate that the entire morphology of the 1DPC is perturbed. Based on the morphological data above (and knowing the thickness values of the layers of

the 1DPC) it is possible to implement a more realistic numerical model. Referring to the unit-cell schematic (with period $\Lambda = 1540$ nm) in Figure 4g, the idealized rectangular on-tip diffraction grating is now replaced by a trapezoidal one, with parameters $h_{bot} = 577$ nm, $b_{bot} = 685$ nm, and $\theta_{bot} = 66°$. In the same way, a trapezoidal shape is assumed on the top, with parameters $h_{top} = 207$ nm, $b_{top} = 350$ nm, and $\theta_{top} = 17°$. By assuming a linear decrease for h, b, and θ from the bottom to the top of the 1DPC along the different layers, we simulated the resulting geometry by means of the finite-element-based commercial software COMSOL Multiphysics (RF module) (see the Supporting Information for details), by assuming the unit cell in Figure 4h.

The simulated (average) spectrum is shown in Figure 4d (red-solid curve), from which we observe a significantly improved agreement with the experimental results, with a visible resonant dip located near the experimental counterpart, and good resemblance in terms of both reflectance values and spectral shapes in the wavelength range of investigation.

In particular, our attained experimental resonance has a Q-factor of ≈ 50, which is more than one order of magnitude lower than the theoretical one pertaining to the idealized configuration in Figure 3a. Though being severely limited by the relief-propagation, the attained value is still larger than most values (within the range from ≈ 15 to ≈ 40) exhibited by recent plasmonic lab-on-tip probes operating in the near infrared.[29,33,44,46]

To finally evaluate the impact of the discussed fabrication tolerance on the sensing characteristics of the attained BSW resonance, we characterized the fabricated structure by measuring its surface sensitivity.[17,30,33] Taking into account the reduced field enhancement attainable at the surface of the 1DPC, the samples were coated with a thin high-RI layer, namely, a 50 nm thick zinc sulfide (ZnS, with RI ≈ 2.27) layer deposited via thermal evaporation (see the Supporting Information).

The spectrum acquired by illuminating the reference sample with the supercontinuum broadband source after the deposition of the ZnS overlay is shown in **Figure 5**a (red curve), and is compared with the counterpart measured before the deposition, previously shown in Figure 4c (blue curve). As it can be observed, the overlay deposition induces expectable redshifts of the dips/peaks arising in the interrogation range, without significant perturbations of the original spectral shapes.

The shifts measured for all the spectral features (labeled in Figure 4a), and the related surface sensitivities are reported in **Table 1** (second and third column). As it can be observed, there is a sensitivity enhancement in the spectral region of interest, with a maximum value of 1.22 nm nm^{-1} obtained at point d, that is, at the dip identified as a signature of the BSW excitation (see the Supporting Information for more details). Specifically, the average sensitivity enhancement at the dip d, evaluated as $E_d = (S_d/3)(S_a^{-1} + S_b^{-1} + S_c^{-1})$ (where S_a, S_b, and S_c are the sensitivities of the features a, b, and c, respectively) is of ≈ 1.38.

We point out that the deposition of the ZnS overlay induces a shift of the spectral feature of interest within the range 1650–1700 nm, which is not covered by the polarized optical source available. Nonetheless, we still carried out polarization measurements (see the Supporting Information), and verified a negligible influence of the light polarization on the spectral locations of all the observable spectral features, both before and
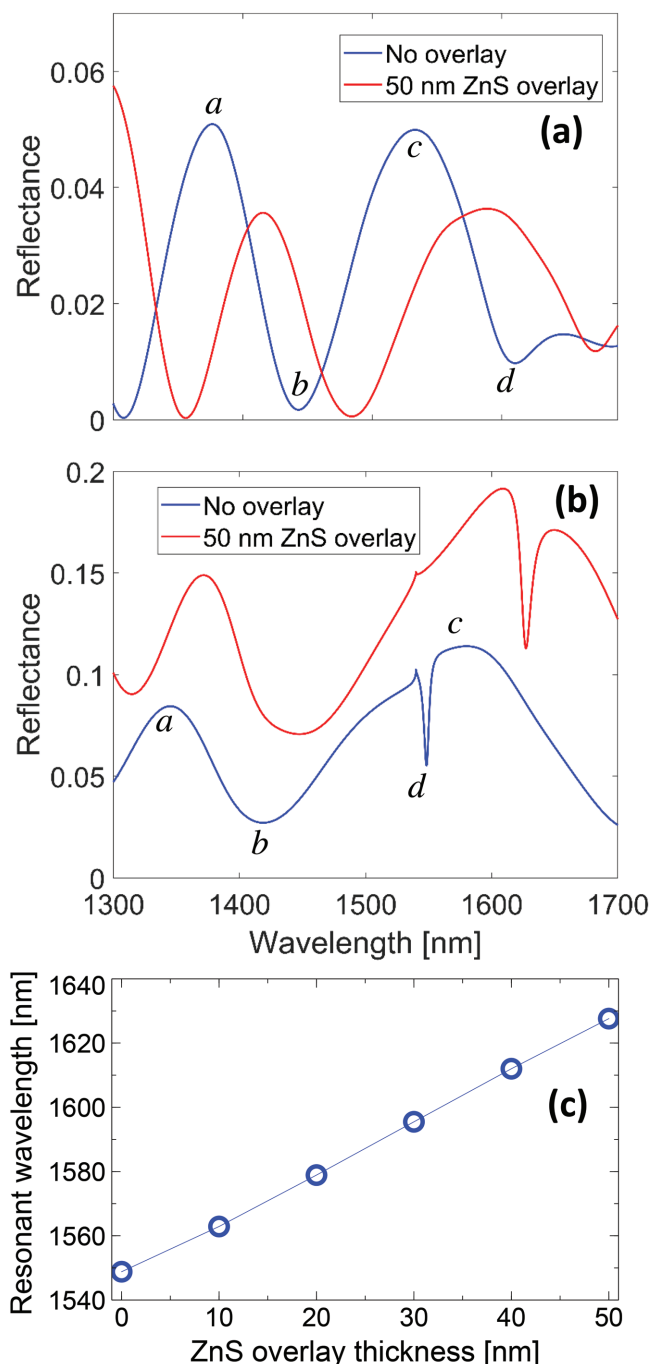
Figure 5. a) Reflectance spectra measured before and after the deposition of a 50-nm-thick ZnS overlay with a broadband supercontinuum source. b) Numerical (average) reflectance spectra, computed by considering the ideal structure in Figure 3a, with and without a 50 nm thick ZnS overlay on the top of 1DPC. The labeled spectral features (dips/peaks) undergo expectable redshifts due to the local RI increase. c) Numerically estimated BSW wavelength (pertaining to the spectral dip labeled as *d*) as a function of the ZnS overlay thickness. The continuous line is a guide to the eye only.

after the overlay deposition. Therefore, the wavelength shifts and surface-sensitivity values reported in Table 1, though pertaining to an unpolarized source, represent valid estimates of the sensitivity behavior of the sample.

Table 1. Wavelength shifts $\Delta\lambda$ and surface sensitivities S_S of the spectral features labeled in Figures 5a,b (see blue curves). Experimental and numerical results pertain to the structures in Figures 4c and 3a, respectively, in the presence and absence of a 50 nm ZnS overlay.

Spectral features	Experimental		Numerical (ideal)	
	$\Delta\lambda$ [nm]	S_S [nm nm^{-1}]	$\Delta\lambda$ [nm]	S_S [nm nm^{-1}]
A	41.1	0.82	25.7	0.51
B	39.8	0.80	27.5	0.55
C	54.0	1.08	38.2	0.76
D	61.1	1.22	79.4	1.59

We now compare the attained results with the numerical predictions pertaining to the idealized structure in Figure 3a (see Figure 5b, and the third and fourth columns of Table 1). Specifically, Figure 5b shows the average spectra computed with and without the ZnS overlay on the surface of the 1DPC (see the Supporting Information for details). Clearly, there is a much higher sensitivity enhancement at the resonant dip ($E_d \approx 2.69$), due to the highly increased spectral selectivity of the resonant phenomenon with respect to the experimental case. Nevertheless, the experimental surface sensitivity is only 1.3 times smaller than the computed value of 1.59 nm nm^{-1}. Therefore, while the relief-propagation phenomenon induces a significant degradation effect of the resonance bandwidth, the observed resonance preserves a high sensitivity, close to the theoretical upper bound. Moreover, we numerically investigated the wavelength shift as a function of the overlay thickness within the thickness range 0–50 nm, which covers most of the relevant biomolecules of practical interest in biosensing applications. As it can be observed in Figure 5c, this relationship is essentially linear, thereby suggesting that the measured surface sensitivity represents a meaningful figure of merit.

Although its primary goal was to provide a proof-of-principle demonstration of BSW excitation, the analyzed structure exhibits a surface sensitivity in line with other plasmonic lab-on-tip probes, such as hybrid metallo-dielectric structures[44] and plasmonic metasurfaces,[33] as summarized in **Table 2**. In particular, the optical fiber meta-tip, which already outperforms traditional plasmonic benchmarks,[33] exhibits a surface sensitivity moderately higher than the BSW structure. However, this is accompanied by an ≈3.3 times lower Q-factor of 15. Within this context, specific optimization strategies aimed at strongly narrowing the resonance linewidth could yield a sensible increase of the maximum FOM reachable by a lab-on-tip BSW probe.

Table 2. Experimental surface sensitivities S_S pertaining to the structure in Figure 4c and other two lab-on-tip plasmonic probes. Notice the different values of the overlay thickness and RI.

Ref.	Fiber tip structure	Overlay specifications	S_S [nm nm^{-1}]
This study	BSW	50 nm ZnS RI ≈ 2.27	1.22
[44]	Hybrid metallo-dielectric	100 nm SiO$_2$ RI ≈ 1.45	0.35
[33]	Meta-tip	40 nm SiO$_x$ RI ≈ 1.70	5.6

**ADVANCED
SCIENCE NEWS**

www.advancedsciencenews.com

**ADVANCED
OPTICAL
MATERIALS**

www.advopticalmat.de

3. Conclusions

To sum up, we have provided the first demonstration of BSW excitation on the fiber tip via grating coupling, and have addressed the practical feasibility of a BSW-based fiber-optic optrode.

More specifically, we have explored, numerically and experimentally, two complementary configurations differing by the position of the grating (either on top of the 1DPC or on the fiber tip), and have carefully investigated the role played by key nonidealities, including optical losses, finite-size effects and, most notably for the on-tip grating configuration, the relief-propagation effects. Of the two configurations, only the on-tip grating one leads to the actual experimental observation of a BSW, though accompanied by an undesirable resonance broadening mainly attributable to the relief-propagation effects. Nevertheless, the measured Q-factor of ≈ 50 is still higher than those (ranging in the interval $[\approx 15, \approx 40]$) typical of current plasmonic lab-on-tip optrodes. Moreover, with a view toward label-free biosensing applications, we also demonstrated a negligible impact of the discussed nonidealities on the sensing characteristics of the platforms.

Indeed, we evaluated a surface sensitivity of 1.22 nm nm^{-1} of deposited ZnS, only 1.3 times smaller than the theoretical upper bound. This value is in line with typical plasmonic benchmarks, even though our proof-of-principle prototype structure was not specifically optimized in this respect.

The observed polarization dependence as well as the surface-sensitivity enhancement at the prescribed wavelength are consistent with the frustrated excitation of a BSW, and cannot be simply attributed to 1DPC-related effects.

Overall, we believe that this work represents a first important step toward the realization of advanced "all-dielectric" fiber-tip probes. Indeed, the reported results also highlight the main challenges to face in order to optimize the proposed platform. In particular, specific efforts need to be mainly focused on narrowing the attainable BSW resonance. Within this context, of the two configurations analyzed, the one with the surface diffraction grating is more robust in terms of fabrication tolerances, but it seems too inefficient in terms of light coupling/collection to enable the excitation of a BSW. In a complementary way, the on-tip grating configuration led to a successful BSW excitation test, but the room for further optimization seems limited in view of the unavoidable impact of the relief-propagation phenomenon. For this reason, future strategies could be aimed at combining the benefits of the two discussed platforms, judiciously evaluating possible follow-up configurations.

More specifically, design modifications to the on-tip grating platform should be explored, in order to substantially mitigate the associated detrimental effects. For instance, reliefless technological solutions based on volume-phase holographic gratings could represent an attractive scenario, which may also endow dramatic improvements in the diffraction efficiency (approaching 100%) and low polarization sensitivity.[47,48] Along the lines of ref. [33], on-tip dielectric metasurfaces could also be explored to attain efficient beam-steering effects with minimal relief propagation effects in view of their low-profile character. These approaches are currently being pursued and will be reported in forthcoming publications.

As for the surface diffraction grating configuration, efforts should be devoted to strongly mitigate finite-size effects. Within this framework, sensible benefits could be obtained via structural modifications similar to those adopted in ref. [43] for confining the in-plane extension of guided-mode resonances. To this aim, the possibility to "open" bandgaps in the BSW dispersion relation could be exploited,[49,50] thereby enabling local trapping of the SW via Bragg reflection phenomena.

[1] J. Polo, T. Mackay, A. Lakhtakia, *Electromagnetic Surface Waves: A Modern Perspective*, Elsevier, Amsterdam **2013**.

[2] J. Zenneck, *Ann. Phys.* **1907**, *328*, 846.

[3] S. A. Maier, *Plasmonics: Fundamentals and Applications*, Springer, Berlin **2007**.

[4] J. Homola, *Chem. Rev.* **2008**, *108*, 462.

[5] R. B. Schasfoort, *Handbook of Surface Plasmon Resonance*, Royal Society of Chemistry, London **2017**.

[6] M. Piliarik, J. Homola, *Opt. Express* **2009**, *17*, 16505.

[7] O. Takayama, L.-C. Crasovan, S. K. Johansen, D. Mihalache, D. Artigas, L. Torner, *Electromagnetics* **2008**, *28*, 126.

[8] Z. Jacob, E. E. Narimanov, *Appl. Phys. Lett.* **2008**, *93*, 221109.

[9] M. U. Khan, B. Corbett, *Sci. Technol. Adv. Mater.* **2016**, *17*, 398.

[10] M. Kaliteevski, I. Iorsh, S. Brand, R. A. Abram, J. M. Chamberlain, A. V. Kavokin, I. A. Shelykh, *Phys. Rev. B* **2007**, *76*, 165415.

[11] D. P. Pulsifer, M. Faryad, A. Lakhtakia, *Phys. Rev. Lett.* **2013**, *111*, 243902.

[12] F. Giorgis, E. Descrovi, C. Summonte, L. Dominici, F. Michelotti, *Opt. Express* **2010**, *18*, 8087.

[13] A. Sinibaldi, E. Descrovi, F. Giorgis, L. Dominici, M. Ballarini, P. Mandracci, N. Danz, F. Michelotti, *Biomed. Opt. Express* **2012**, *3*, 2405.

[14] A. Sinibaldi, N. Danz, E. Descrovi, P. Munzert, U. Schulz, F. Sonntag, L. Dominici, F. Michelotti, *Sens. Actuators B* **2012**, *174*, 292.

[15] A. Sinibaldi, R. Rizzo, G. Figliozzi, E. Descrovi, N. Danz, P. Munzert, A. Anopchenko, F. Michelotti, *Opt. Express* **2013**, *21*, 23331.

[16] A. Sinibaldi, A. Fieramosca, R. Rizzo, A. Anopchenko, N. Danz, P. Munzert, C. Magistris, C. Barolo, F. Michelotti, *Opt. Lett.* **2014**, *39*, 2947.

[17] R. Rizzo, N. Danz, F. Michelotti, E. Maillart, A. Anopchenko, C. Wächter, *Opt. Express* **2014**, *22*, 23202.

[18] Y. Guo, J. Y. Ye, C. Divin, B. Huang, T. P. Thomas, J. R. Baker Jr., T. B. Norris, *Anal. Chem.* **2010**, *82*, 5211.

[19] V. Paeder, V. Musi, L. Hvozdara, S. Herminjard, H. P. Herzig, *Sens. Actuators B* **2011**, *157*, 260.

[20] A. Farmer, A. C. Friedli, S. M. Wright, W. M. Robertson, *Sens. Actuators B* **2012**, *173*, 79.

[21] P. Rivolo, F. Michelotti, F. Frascella, G. Digregorio, P. Mandracci, L. Dominici, F. Giorgis, E. Descrovi, *Sens. Actuators B* **2012**, *161*, 1046.

[22] V. N. Konopsky, T. Karakouz, E. V. Alieva, C. Vicario, S. K. Sekatskii, G. Dietler, *Sensors* **2013**, *13*, 2566.

[23] G. A. Rodriguez, J. D. Ryckman, Y. Jiao, S. M. Weiss, *Biosens. Bioelectron.* **2014**, *53*, 486.

[24] F. Frascella, C. Petri, S. Ricciardi, L. Napione, P. Munzert, U. Jonas, J. Dostalek, F. Bussolino, C. F. Pirri, E. Descrovi, *J. Light Technol.* **2016**, *34*, 3641.

[25] A. Sinibaldi, C. Sampaoli, N. Danz, P. Munzert, L. Sibilio, F. Sonntag, A. Occhicone, E. Falvo, E. Tremante, P. Giacomini, F. Michelotti, *Biosens. Bioelectron.* **2017**, *92*, 125.

[26] R. Dubey, E. Barakat, M. Häyrinen, M. Roussey, S. K. Honkanen, M. Kuittinen, H. P. Herzig, *J. Eur. Opt. Soc. Rapid Publ.* **2017**, *13*, 5.

[27] V. Koju, W. M. Robertson, *Sci. Rep.* **2017**, *7*, 3233.

[28] M. Scaravilli, G. Castaldi, A. Cusano, V. Galdi, *Opt. Express* **2016**, *24*, 27771.

[29] M. Consales, A. Ricciardi, A. Crescitelli, E. Esposito, A. Cutolo, A. Cusano, *ACS Nano* **2012**, *6*, 3163.

[30] A. Cusano, M. Consales, A. Crescitelli, A. Ricciardi, *Lab-on-Fiber Technology*, Springer, Berlin **2014**.

[31] A. Ricciardi, A. Crescitelli, P. Vaiano, G. Quero, M. Consales, M. Pisco, E. Esposito, A. Cusano, *Analyst* **2015**, *140*, 8068.

[32] P. Vaiano, B. Carotenuto, M. Pisco, A. Ricciardi, G. Quero, M. Consales, A. Crescitelli, A. Esposito, A. Cusano, *Laser Photonics Rev.* **2016**, *10*, 922.

[33] M. Principe, M. Consales, A. Micco, A. Crescitelli, G. Castaldi, A. Esposito, V. La Ferrara, A. Cutolo, V. Galdi, A. Cusano, *Light: Sci. Appl.* **2017**, *6*, e16226.

[34] M. Pisco, F. Galeotti, G. Quero, G. Grisci, A. Micco, L. V. Mercaldo, P. Delli Veneri, A. Cutolo, A. Cusano, *Light: Sci. Appl.* **2017**, *6*, e16229.

[35] S. Li, J. Liu, Z. Zheng, Y. Wan, W. Kong, Y. Sun, *IEEE Sens. J.* **2016**, *16*, 1200.

[36] X. J. Tan, X. S. Zhu, *Opt. Express* **2016**, *24*, 16016.

[37] T. Tu, F. Pang, S. Zhu, J. Cheng, H. Liu, J. Wen, T. Wang, *Opt. Express* **2017**, *25*, 9019.

[38] M. G. Moharam, T. K. Gaylord, E. B. Grann, D. A. Pommet, *J. Opt. Soc. Am. A* **1995**, *12*, 1068.

[39] M. G. Moharam, T. K. Gaylord, D. A. Pommet, E. B. Grann, *J. Opt. Soc. Am. A* **1995**, *12*, 1077.

[40] F. C. Tai, S. C. Lee, J. Chen, C. Wei, S. H. Chang, *J. Raman Spectrosc.* **2009**, *40*, 1055.

[41] A. Micco, A. Ricciardi, M. Pisco, V. La Ferrara, A. Cusano, *Sci. Rep.* **2015**, *5*, 15935.

[42] A. Aliberti, A. Ricciardi, M. Giaquinto, A. Micco, E. Bobeico, V. La Ferrara, M. Ruvo, A. Cutolo, A. Cusano, *Sci. Rep.* **2017**, *7*, 14459.

[43] J. O. Grepstad, M. M. Greve, B. Holst, I. R. Johansen, O. Solgaard, A. Sudbø, *Opt. Express* **2013**, *21*, 23640.

[44] A. Ricciardi, M. Consales, G. Quero, A. Crescitelli, E. Esposito, A. Cusano, *ACS Photonics* **2013**, *1*, 69.

[45] Y. Lin, Y. Zou, R. G. Lindquist, *Biomed. Opt. Express* **2011**, *2*, 478.

[46] M. Pisco, F. Galeotti, G. Quero, A. Iadicicco, M. Giordano, A. Cusano, *ACS Photonics* **2014**, *1*, 917.

[47] R. R. A. Syms, *Practical Volume Holography*, Oxford University Press, Oxford **1990**.

[48] G. Bianco, M. A. Ferrara, F. Borbone, A. Roviello, V. Pagliarulo, S. Grilli, P. Ferraro, V. Striano, G. Coppola, *Proc. SPIE* **2015**, *9508*, 950807.

[49] E. Descrovi, F. Giorgis, L. Dominici, F. Michelotti, *Opt. Lett.* **2008**, *33*, 243.

[50] T. Sfez, E. Descrovi, L. Dominici, W. Nakagawa, F. Michelotti, F. Giorgis, H. P. Herzig, *Appl. Phys. Lett.* **2008**, *93*, 061108.

1800477 (10 of 10)